

Demonstration of Unusual Thermal Effect in the Casimir Force from Graphene

M. Liu,¹ Y. Zhang,¹ G. L. Klimchitskaya,^{2,3} V. M. Mostepanenko,^{2,3,4} and U. Mohideen^{*1}

¹*Department of Physics and Astronomy, University of California, Riverside, California 92521, USA*

²*Central Astronomical Observatory at Pulkovo of the Russian Academy of Sciences, Saint Petersburg, 196140, Russia*

³*Institute of Physics, Nanotechnology and Telecommunications,*

Peter the Great Saint Petersburg Polytechnic University, Saint Petersburg, 195251, Russia

⁴*Kazan Federal University, Kazan, 420008, Russia*

We report precision measurements of the gradient of the Casimir force between an Au-coated sphere and graphene sheet deposited on a silica plate. The measurement data are compared with exact theory using the polarization tensor found in the framework of the Dirac model including effects of the nonzero chemical potential and energy gap of the graphene sample with no fitting parameters. The very good agreement between experiment and theory demonstrates the unusually big thermal effect at separations below 1 μm which has never been observed for conventional 3D materials. Thus, it is confirmed experimentally that for graphene the effective temperature is determined by the Fermi velocity rather than by the speed of light.

Over the last two decades special attention has been given to graphene which is a 2D sheet of carbon atoms packed in a hexagonal lattice. The quasiparticles in graphene are either massless or very light. At energies up to a few eV they are well described by the relativistic Dirac equation in 2+1 dimensions where the speed of light c is replaced with the Fermi velocity $v_F \approx c/300$ [1–3]. As a result, graphene offers many advantages over conventional materials with regard to its mechanical, electrical, optical, and chemical properties. It possesses the universal minimum electrical conductivity, low absorbance in the range from visible to infrared light and extremely high mechanical strength [1–3].

One more outstanding feature is an unusually big thermal correction to the Casimir force between two parallel graphene sheets spaced at separations below 1 μm which was predicted by G. Gómez-Santos [4]. In general, the Casimir force [5] acts between any two closely spaced surfaces. It is a generalization of the commonly known van der Waals force [6] taking into account the finite speed of light. Both forces are of entirely quantum nature. They are caused by the zero-point and thermal fluctuations of the electromagnetic field. Since fluctuations have a profound impact in many physical phenomena, the Casimir effect has gained recognition as one of the multidisciplinary areas of current research (see, e.g., the reviews [7–11] and monographs [12–18]).

The Casimir force is described by the fundamental Lifshitz theory [19, 20]. The force value at temperature T can be presented as the zero-temperature contribution plus a thermal correction. For two parallel plates made of 3D materials spaced at separations $a < 1 \mu\text{m}$, $T = 300 \text{ K}$ the thermal correction to the Casimir force is very small and is not yet measured. The reason is that $T \ll T_{\text{eff}} = \hbar c/(2ak_B) \approx 1140 \text{ K}$ at $a = 1 \mu\text{m}$.

It becomes equal to a sizable fraction of the force only at separations of a few micrometers where the force itself is too small. It should be noted that a metal described by the Drude model is an exception [21], but the few percent thermal effect predicted in this case at $a < 1 \mu\text{m}$ was unambiguously excluded experimentally [22, 23]. There is an extensive literature regarding the reasons for this exclusion but the problem remains as yet unresolved [8, 11, 16, 23] (see also a recent overview and a novel approach in Ref. [24]). Quite apart from the case of 3D bodies, according to the prediction of Ref. [4], for two pristine graphene sheets (undoped and with massless quasiparticles) the thermal correction to the Casimir force at $T = 300 \text{ K}$ becomes large even at separations of tens of nanometers. This is because for graphene $T_{\text{eff}}^{(g)} = \hbar v_F/(2ak_B) \approx T_{\text{eff}}/300$ [4]. By introducing the thermal photon wavelength $\lambda_T = 2\pi\hbar c/(k_B T) \approx 4.8 \mu\text{m}$ at $T = 300 \text{ K}$, one finds that for a pristine graphene the high-temperature regime takes place at $a \geq \lambda_T/(1200\pi) \approx 1.3 \text{ nm}$.

In this Letter, we present the measurement results for the gradient of the Casimir force between an Au-coated microsphere and a graphene sheet deposited on a silica glass (SiO_2) plate obtained in high vacuum using an atomic force microscope (AFM) operated in the dynamic regime. Although for two parallel graphene sheets suspended in a vacuum the thermal correction at short separations reaches several tens percent of the Casimir force [4, 25], this configuration is experimentally not feasible. In the previously performed experiment [26] using a graphene sheet deposited on a SiO_2 film covering a Si plate, the gradient of the Casimir force was measured and found in good agreement with theory [27]. However, the thermal effect could not be discriminated because the charge carrier concentration in a Si plate was burdened with a large error and the used theory did not take into account that real graphene samples are unavoidably doped. In the present experiment, an improved AFM setup and a much thicker SiO_2 substrate (as suggested

*Umar.Mohideen@ucr.edu

in Ref. [28]) are used. We have also removed the Si plate and made a comparison with exact theory taking into account the nonzero chemical potential and energy gap of the graphene sample. As a result, the measured gradients of the Casimir force were found to be in a very good agreement with theory and the thermal effect was reliably demonstrated in the separation range from 250 to 590 nm where it constitutes from 4% to 10% of the total force gradient.

The Casimir force gradient measurement system consists of a tipless AFM cantilever [29] whose spring constant was reduced through chemical etching before use. The corresponding cantilever resonant frequency was decreased from 5.7579×10^4 to 3.5286×10^4 rad/s by etching for 100 s in 60% KOH solution at 75°C with stirring. The cantilever was washed in BOE solution and DI water for 1 min each prior to etching. The etching process reduced the spring constant of the bare cantilever to 0.008327 N/m. As in previous experiments, a hollow glass microsphere was next attached to the end of the cantilever using silver epoxy and then coated with Au. The thickness of the Au coating and the diameter of the coated sphere were measured to be 120 ± 3 nm and 120.7 ± 0.1 μm using an AFM and a scanning electron microscope, respectively. The rms roughness of the Au coating was measured to be $\delta_s = 0.9 \pm 0.1$ nm. The resonant frequency of the complete Au coated cantilever-sphere system was measured in vacuum to be $\omega_0 = 6.1581 \times 10^3$ rad/s.

The large area graphene monolayer [30] originally CVD grown on a Cu foil was transferred onto a polished JGS2 grade fused silica double side optically polished substrate of 100 mm diameter and thickness of 500 μm [31] through an electrochemical delamination procedure [30, 32]. A 1×1 cm^2 piece of the graphene coated fused silica wafer was then cut from the large sample and used in the experiment. The roughness of the graphene on the fused silica substrate was measured using an AFM to be $\delta_g = 1.5 \pm 0.1$ nm after the force gradient measurements.

The graphene impurity concentration was determined after the Casimir force gradient measurement utilizing Raman spectroscopy, which was carried out using a Horiba Labram HR 800 system with 532 nm laser excitation (Laser Quantum, 65 mW power). A 100x objective lens with NA = 0.9 was used, which leads to a laser spot size of $\sim 0.4 \mu\text{m}^2$ (i.e., of 709 nm diameter). Experiments were performed at $T = 294 \pm 0.5$ K. A 600 1/m grating was used to ensure the spectral range of interest (from 1450 cm^{-1} to 2900 cm^{-1}) which includes both G and 2D disorder peaks of graphene. Before collection of spectra at each position, the signal intensity was maximized in real-time by adjusting the focus of the microscope, so that graphene sample was located in the focal plane. The spectrometer calibration was performed as per manual by reflecting the incident light. Spectral resolution for G peak identification was measured to be 0.1 cm^{-1} .

The spectra collected are integrated results of 10 acquisitions with each acquisition spanning over 10 s. The spectra were fit to Lorentzians to identify the G-peak. The G-peak value was compared to reported G-peak shifts with charge concentration in Ref. [33] to identify the impurity concentration in graphene. The latter was measured at 18 different uniformly distributed locations on the sample to arrive at an average impurity concentration of $n = (4.2 \pm 0.3) \times 10^{12} \text{ cm}^{-2}$ where the random and systematic errors are summed to obtain the maximum possible value of the total error. The dominant impurity chemical type was Na resulting from the transfer process used [30]. The respective zero-temperature value of the chemical potential for our sample is given by [34] $\mu = \hbar v_F \sqrt{\pi n} = 0.24 \pm 0.01$ eV. This value is relatively large and, thus, almost independent of T [35]. Regarding the energy gap Δ , for graphene on a SiO_2 substrate its values vary between 0.01 and 0.2 eV [36–40].

Specifics of the vacuum chamber setup have been reported in detail in previous publications [41–44]. The schematic is provided in Fig. 1 of Ref. [44]. The fused silica-supported graphene sample and gold sphere probe were loaded into the vacuum chamber which was pumped down to below 9×10^{-9} Torr using an oil free scroll pump and turbo pump prior to the force gradient measurements. Due to the sensitive nature of the graphene sample, the UV/Ar-ion radiation treatment used in previous experiments [42–45] for cleaning the Au surfaces was not implemented to avoid potential damage to the atomic layer graphene. The cantilever oscillation frequency and motion of the graphene surface were monitored by two fiber interferometers with 1550 nm and 500.1 nm laser light sources, respectively. A small separation distance change originating from mechanical drifts during the time span of the measurements were also taken into consideration. Details of the above mentioned operations and mechanisms are explained in Refs. [41, 43, 44]. The gradient of the Casimir force was measured using a dynamic technique, where the force-induced frequency-shift of cantilever oscillation is directly taken using a phase lock loop (PLL) [41]. The cantilever oscillation amplitude was maintained at 10 nm and the PLL resolution was measured to be 55.3 mrad/s. To ensure the accuracy of the measurement, the residual potential difference between the gold and graphene surface was determined through a standard electrostatic calibration procedure [41, 43, 44].

In the dynamic measurement scheme used here, the total force $F_{\text{tot}}(a) = F_{\text{el}}(a) + F(a)$ acting on the Au coated sphere, where $F_{\text{el}}(a)$ and $F(a)$ are the electric and Casimir force, respectively, and a is the separation distance between the sphere and graphene, modifies the resonant natural frequency of the cantilever-sphere oscillator system. The change in the frequency $\Delta\omega = \omega_r - \omega_0$, where ω_r is the resonance frequency in the presence of external force $F_{\text{tot}}(a)$, was recorded by the PLL every

0.14 nm while the graphene plate was moved towards the grounded sphere starting at the maximum separation. This was repeated with one of ten different voltages V_i varied between 0.083 and 0.183 V and eleven voltages equal to the residual potential difference V_0 (see below) applied to the graphene using ohmic contacts while the sphere remained grounded.

The gradients of the total and Casimir forces were found from the measured frequency shifts using electrostatic calibration. To perform the calibration of the setup, we used an expression for the electric force in sphere-plate geometry $F_{\text{el}}(a) = X(a, R)(V_i - V_0)^2$. Here, $X(a, R)$ is a known function [16, 44] and V_0 is the residual potential difference between a sphere and a graphene sheet which is nonzero even when both surfaces are grounded. In the linear regime realized in our measurement the gradient of the Casimir force is given by [44]

$$F'(a) = -\frac{\Delta\omega}{C} - (V_i - V_0)^2 \frac{\partial X(a, R)}{\partial a}, \quad (1)$$

where $C = \omega_0/(2k)$ and k is the spring constant of the cantilever. Note that the absolute separations between the zero levels of the roughness on the sphere and graphene are found from $a = z_{\text{piezo}} + z_0$, where z_{piezo} is the graphene plate movement due to the piezoelectric actuator and z_0 is the closest approach between the Au sphere and graphene.

From the position of the maximum in the parabolic dependence of $\Delta\omega$ on V_i in Eq. (1), one can determine V_0 with the help of a χ^2 -fitting procedure. From the curvature of the parabola with the help of the same fit it is possible to determine z_0 and C . This was done at all the graphene-Au sphere separations used in our experiment. In Fig. 1 we present the values of V_0 as a function of separation determined from the fit. The obtained values were corrected for mechanical drift of the frequency-shift signal, as discussed in Refs. [41, 43, 44]. As can be seen from Fig. 1, the resulting values of V_0 do not depend on separation. To check this observation, we have performed the best fit of V_0 to the straight lines $V_0 = d + \theta a$ where a is measured in nanometers. It was found that $d = 0.1326$ V and the slope is $\theta = -2.73 \times 10^{-7}$ V/nm, i.e., the independence of V_0 on a was confirmed to a high precision. This finally leads to the mean value $V_0 = 0.1324$ V. Next the quantities z_0 and C were determined from the fit at different separations and found to be separation independent. For our graphene sample the mean values were found to be $z_0 = 236.9 \pm 0.6$ nm and $C = (1.464 \pm 0.001) \times 10^5$ s/kg. From the measured resonant frequency we have confirmed that the obtained value of C results in the spring constant k consistent with the value determined prior to the Au coating of the cantilever.

At each separation, the gradient of the Casimir force

was measured 21 times with different applied voltages mentioned above. The mean values of the gradient of

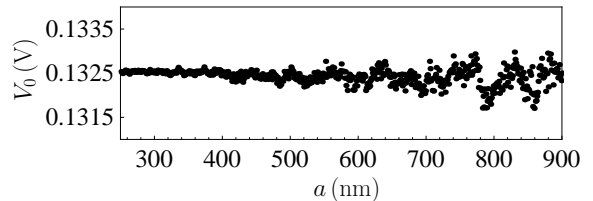


FIG. 1: The residual potential difference between a Au-coated sphere and a graphene sample is shown by the dots as a function of separation.

the Casimir force were found from Eq. (1) with a step of 1 nm. The random errors of the mean were determined at a 67% confidence level and combined in quadrature with the systematic errors which are mostly determined by the errors in measuring the frequency shifts. The obtained measurement data for $F'_{\text{expt}}(a)$ with their errors are shown in Fig. 2 as crosses where $\Delta a = 0.6$ nm [for visual clarity in Fig. 2(a) all data points are indicated whereas in Figs. 2(b,c) each second data point and in Fig. 2(d) only each third one are shown].

Now we compare the measurement results with theory. In Ref. [4], the Casimir force in graphene systems was calculated using the density-density correlation functions in the random-phase approximation (see also [46]). This formalism is equivalent to the nonretarded version of the Lifshitz theory (in so doing, the relativistic effects were shown to be insignificant [4]). Here, we use the relativistic version of the Lifshitz formula with reflection coefficients expressed via the exact polarization tensor of graphene in the framework of the Dirac model taking into account the nonzero energy gap Δ and chemical potential μ [47–50]. Note that even at the shortest separation considered ($a = 250$ nm) the characteristic energy of the Casimir effect $\hbar\omega_c = \hbar c/(2a) = 0.4$ eV is well within the application region of the Dirac model. Because of this the absorption peak of graphene at $\lambda = 270$ nm ($\hbar\omega = 2\pi\hbar c/\lambda \approx 4.59$ eV) does not influence the obtained results. Then, using the proximity force approximation (PFA) [16], the gradient of the Casimir force acting between a Au sphere of radius R and a graphene-coated SiO_2 plate spaced at the separation a at temperature T is given by [25, 27]

$$F'(a, T) = 2k_B T R \sum_{l=0}^{\infty} ' \int_0^{\infty} q_l k_{\perp} dk_{\perp} \times \sum_{\alpha} [r_{\alpha}^{-1}(i\xi_l, k_{\perp}) R_{\alpha}^{-1}(i\xi_l, k_{\perp}) e^{2aq_l} - 1]^{-1}. \quad (2)$$

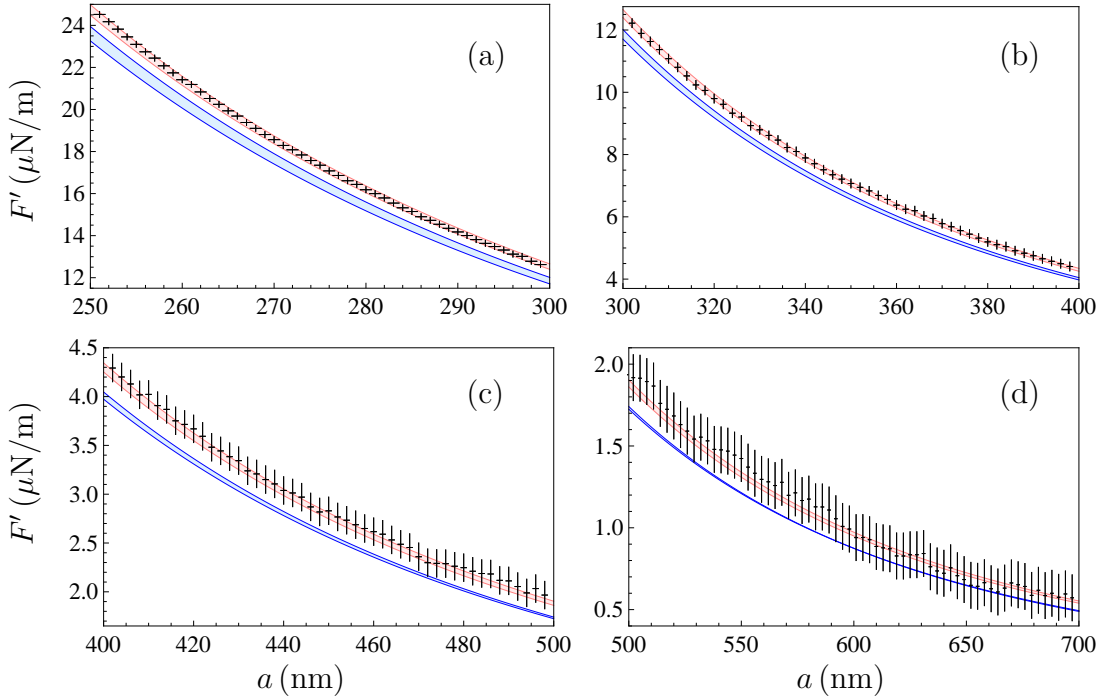


FIG. 2: The mean gradient of the Casimir force is shown by the crosses as a function of separation. The top and bottom theoretical bands are computed at $T = 294$ K and 0 K, respectively (see the text for further discussion).

Here, the prime on the summation sign in l divides the term with $l = 0$ by 2, k_{\perp} is the magnitude of the wave vector projection on the graphene, $\xi_l = 2\pi k_B T l / \hbar$ are the Matsubara frequencies, $q_l = \sqrt{k_{\perp}^2 + \xi_l^2 / c^2}$, and the summation in α is over the transverse magnetic ($\alpha = \text{TM}$) and transverse electric ($\alpha = \text{TE}$) polarizations of the electromagnetic field (note that the thicknesses of Au coating and SiO₂ plate allow consideration of a sphere as all-gold and a plate as a semispace [16]). The reflection coefficients r_{α} on the boundaries between Au and vacuum and R_{α} between vacuum and graphene-coated plate are given by [25, 27, 51]

$$\begin{aligned} r_{\text{TM}}(i\xi_l, k_{\perp}) &= \frac{\varepsilon_l^{(1)} q_l - k_l^{(1)}}{\varepsilon_l^{(1)} q_l + k_l^{(1)}}, \quad r_{\text{TE}}(i\xi_l, k_{\perp}) = \frac{q_l - k_l^{(1)}}{q_l + k_l^{(1)}}, \\ R_{\text{TM}}(i\xi_l, k_{\perp}) &= \frac{\hbar k_{\perp}^2 (\varepsilon_l^{(2)} q_l - k_l^{(2)}) + q_l k_l^{(2)} \Pi_{00,l}}{\hbar k_{\perp}^2 (\varepsilon_l^{(2)} q_l + k_l^{(2)}) + q_l k_l^{(2)} \Pi_{00,l}}, \\ R_{\text{TE}}(i\xi_l, k_{\perp}) &= \frac{\hbar k_{\perp}^2 (q_l - k_l^{(2)}) - \Pi_l}{\hbar k_{\perp}^2 (q_l + k_l^{(2)}) + \Pi_l}, \end{aligned} \quad (3)$$

where $\varepsilon_l^{(n)} = \varepsilon^{(n)}(i\xi_l)$ with $n = 1, 2$ are the dielectric permittivities of Au and SiO₂, respectively, and $k_l^{(n)} = \sqrt{k_{\perp}^2 + \varepsilon_l^{(n)} \xi_l^2 / c^2}$. The components of the polarization tensor of graphene are $\Pi_{\beta\gamma,l} \equiv \Pi_{\beta\gamma}(i\xi_l, k_{\perp}, T, \Delta, \mu)$, where $\beta, \gamma = 0, 1, 2$, and the combination of these components Π_l is defined as

$$\Pi_l = k_{\perp}^2 \Pi_{\beta,l}^{\beta} - q_l^2 \Pi_{00,l}. \quad (4)$$

It is convenient to present the quantities $\Pi_{00,l}$ and Π_l in the form

$$\Pi_{00,l} = \Pi_{00,l}^{(0)} + \Pi_{00,l}^{(1)}, \quad \Pi_l = \Pi_l^{(0)} + \Pi_l^{(1)}, \quad (5)$$

where the first contributions describe undoped graphene ($\mu = 0$) with a nonzero energy gap ($\Delta = 2mv_F^2$, m is the mass of quasiparticles) at $T = 0$ but with $\omega = i\xi_l$, and the second ones take into account an explicit dependence of the polarization tensor on T and μ . It has been shown that [47, 48]

$$\Pi_{00,l}^{(0)} = \frac{\alpha \hbar k_{\perp}^2}{\tilde{q}_l} \Psi(D_l), \quad \Pi_l^{(0)} = \alpha \hbar \tilde{q}_l \Psi(D_l), \quad (6)$$

where $\tilde{q}_l = \sqrt{v_F^2 k_{\perp}^2 + \xi_l^2} / c$, $\alpha = e^2 / (\hbar c)$ is the fine structure constant, $\Psi(x) = 2[x + (1 - x^2) \arctan(x^{-1})]$, and $D_l = \Delta / (\hbar c \tilde{q}_l)$.

The exact expressions for $\Pi_{00,l}^{(1)}$ and $\Pi_l^{(1)}$ can be found in Refs. [50, 51]

$$\begin{aligned} \Pi_{00,l}^{(1)} &= \frac{4\alpha \hbar c^2 \tilde{q}_l}{v_F^2} \int_{D_l}^{\infty} du \left(\sum_{\kappa=\pm 1} \frac{1}{e^{B_l u + \kappa \frac{\mu}{k_B T}} + 1} \right) \\ &\quad \times \left[1 - \text{Re} \frac{1 - u^2 + 2i\gamma_l u}{(1 - u^2 + 2i\gamma_l u + D_l^2 - \gamma_l^2 D_l^2)^{1/2}} \right], \\ \Pi_l^{(1)} &= -\frac{4\alpha \hbar \tilde{q}_l \xi_l^2}{v_F^2} \int_{D_l}^{\infty} du \left(\sum_{\kappa=\pm 1} \frac{1}{e^{B_l u + \kappa \frac{\mu}{k_B T}} + 1} \right) \\ &\quad \times \left[1 - \text{Re} \frac{(1 + i\gamma_l^{-1} u)^2 + (\gamma_l^{-2} - 1) D_l^2}{(1 - u^2 + 2i\gamma_l u + D_l^2 - \gamma_l^2 D_l^2)^{1/2}} \right], \end{aligned} \quad (7)$$

where $\gamma_l \equiv \xi_l/(c\tilde{q}_l)$ and $B_l \equiv \hbar c\tilde{q}_l/(2k_B T)$.

The values of $\varepsilon_l^{(n)}$ were obtained [8, 16] by means of the Kramers-Kronig relation using the tabulated optical data for Au and SiO₂ [52]. Note that due to the smallness of the reflection coefficient $R_{\text{TE}}(0, k_{\perp})$ the values of force gradients are almost independent of the type of extrapolation of the available optical data for Au down to zero frequency.

The gradients of the Casimir force computed by Eqs. (2)–(7) at $T = 294$ K were corrected (a fraction of 1% effect) for the presence of surface roughness [8, 16]

$$F'_{\text{theor}}(a, T) = \left(1 + 10 \frac{\delta_s^2 + \delta_g^2}{a^2}\right) F'(a, T). \quad (8)$$

The same computations have been repeated at $T = 0$ when the summation on l in Eq. (2) is replaced with integration (the explicit expressions for $\Pi_{00}(i\xi, k_{\perp}, 0, \Delta, \mu)$ and $\Pi(i\xi, k_{\perp}, 0, \Delta, \mu)$ are contained in Ref. [51]).

The computational results for the boundaries of allowed theoretical bands are shown in Fig. 2 by the top and bottom pairs of lines computed at $T = 294$ K and $T = 0$ K, respectively. These lines were obtained in the following most conservative manner. The upper lines in both pairs were computed for $\mu = 0.25$ eV, $\Delta = 0$ eV, whereas the lower lines — for $\mu = 0.23$ eV, $\Delta = 0.2$ eV (we recall that with increasing μ and Δ the force gradient increases and decreases, respectively). Keeping in mind that the PFA slightly increases the force gradients, we did not correct the upper lines for the PFA errors but introduced the maximum possible correction factor of $(1 - a/R)$ to the lower boundary lines [53–57]. The widths of theoretical bands have also been increased to incorporate errors in the sphere radius and optical data of Au and SiO₂.

As is seen in Fig. 2, the measurement data are in excellent agreement with theoretical predictions at $T = 294$ K. The unusual thermal effect in the force gradient equal to the difference between the top and bottom bands is conclusively demonstrated over the region from 250 to 590 nm. Specifically, at $a = 250, 300, 400, 500$, and 590 nm the thermal correction reaches 4%, 5%, 7%, 8.5%, and 10% of the total force gradient, respectively. This correction is smaller than for a pristine graphene because it is suppressed by the relatively large value of μ . The thermal correction is contributed by a summation over the T -dependent Matsubara frequencies and an explicit dependence of the polarization tensor on T as a parameter. For a pristine graphene both effects contribute almost equally [25]. In our case a summation over the Matsubara frequencies contributes 70%, 81%, and 88% of the thermal correction at $a = 250, 400$, and 600 nm, respectively.

To conclude, we demonstrated the unusual thermal effect in the Casimir force from graphene at separations below 1 μm . Although similar effects are the subject of

considerable literature, they have never been observed in measurements of the Casimir interaction at short separations. This result is important not only for the fundamental investigations of graphene and for Casimir physics, but for numerous applications in nanoscale science.

The work of M. L., Y. Z. and U. M. was partially supported by the NSF grant PHY-2012201. The work of G. L. K. and V. M. M. was partially supported by the Peter the Great Saint Petersburg Polytechnic University in the framework of the Russian state assignment for basic research (project N FSEG-2020-0024). V. M. M. was partially funded by the Russian Foundation for Basic Research, Grant No. 19-02-00453 A. His work was also partially supported by the Russian Government Program of Competitive Growth of Kazan Federal University.

-
- [1] A. H. Castro Neto, F. Guinea, N. M. R. Peres, K. S. Novoselov, and A. K. Geim, The electronic properties of graphene, *Rev. Mod. Phys.* **81**, 109 (2009).
 - [2] *Physics of Graphene*, ed. H. Aoki and M. S. Dresselhaus (Springer, Cham, 2014).
 - [3] M. I. Katsnelson, *The Physics of Graphene* (Cambridge University Press, Cambridge, 2020).
 - [4] G. Gómez-Santos, Thermal van der Waals interaction between graphene layers, *Phys. Rev. B* **80**, 245424 (2009).
 - [5] H. B. G. Casimir, On the attraction between two perfectly conducting bodies, *Proc. Kon. Ned. Akad. Wet. B* **51**, 793 (1948).
 - [6] V. A. Parsegian, *Van der Waals Forces: Handbook for Biologists, Chemists, Engineers, and Physicists* (Cambridge University Press, Cambridge, 2005).
 - [7] M. Kardar and R. Golestanian, The “friction” of vacuum, and other fluctuation-induced forces, *Rev. Mod. Phys.* **71**, 1233 (1999).
 - [8] G. L. Klimchitskaya, U. Mohideen, and V. M. Mostepanenko, The Casimir force between real materials: Experiment and theory, *Rev. Mod. Phys.* **81**, 1827 (2009).
 - [9] R. H. French, V. A. Parsegian, R. Podgornik, et al., Long range interactions in nanoscale science, *Rev. Mod. Phys.* **82**, 1887 (2010).
 - [10] A. W. Rodrigues, F. Capasso, and S. G. Johnson, The Casimir effect in microstructured geometries, *Nat. Photon.* **5**, 211 (2011).
 - [11] L. M. Woods, D. A. R. Dalvit, A. Tkatchenko, P. Rodriguez-Lopez, A. W. Rodriguez, and R. Podgornik, Materials perspective on Casimir and van der Waals interactions, *Rev. Mod. Phys.* **88**, 045003 (2016).
 - [12] J. Mahanty and B. W. Ninham, *Dispersion Forces* (Academic Press, London, 1976).
 - [13] P. W. Milonni, *The Quantum Vacuum. An Introduction to Quantum Electrodynamics* (Academic Press, San Diego, 1994).
 - [14] V. M. Mostepanenko and N. N. Trunov, *The Casimir Effect and Its Applications* (Clarendon Press, Oxford, 1997).
 - [15] K. A. Milton, *The Casimir Effect: Physical Manifestations of Zero-Point Energy* (World Scientific, Singapore, 2001).

- [16] M. Bordag, G. L. Klimchitskaya, U. Mohideen, and V. M. Mostepanenko, *Advances in the Casimir Effect* (Oxford University Press, Oxford, 2015).
- [17] S. Y. Buhmann, *Dispersion Forces, I,II* (Springer, Berlin, 2012).
- [18] Bo E. Sernelius, *Fundamentals of van der Waals and Casimir Interactions* (Springer, New York, 2018).
- [19] E. M. Lifshitz, The theory of molecular attractive forces between solids, *Zh. Eksp. Teor. Fiz.* **29**, 94 (1955) [Sov. Phys. JETP **2**, 73 (1956)].
- [20] E. M. Lifshitz and L. P. Pitaevskii, *Statistical Physics, Part II* (Pergamon, Oxford, 1980).
- [21] M. Boström and Bo E. Sernelius, Thermal Effects on the Casimir Force in the $0.15 \mu\text{m}$ Range, *Phys. Rev. Lett.* **84**, 4757 (2000).
- [22] R. S. Decca, D. López, E. Fischbach, G. L. Klimchitskaya, D. E. Krause, and V. M. Mostepanenko, Tests of new physics from precise measurements of the Casimir pressure between two gold-coated plates, *Phys. Rev. D* **75**, 077101 (2007).
- [23] G. Bimonte, D. López, and R. S. Decca, Isoelectronic determination of the thermal Casimir force, *Phys. Rev. B* **93**, 184434 (2016).
- [24] G. L. Klimchitskaya and V. M. Mostepanenko, An alternative response to the off-shell quantum fluctuations: A step forward in resolution of the Casimir puzzle, *Eur. Phys. J. C* **80**, 900 (2020).
- [25] G. L. Klimchitskaya and V. M. Mostepanenko, Origin of large thermal effect in the Casimir interaction between two graphene sheets, *Phys. Rev. B* **91**, 174501 (2015).
- [26] A. A. Banishev, H. Wen, J. Xu, R. K. Kawakami, G. L. Klimchitskaya, V. M. Mostepanenko, and U. Mohideen, *Phys. Rev. B* **87**, 205433 (2013).
- [27] G. L. Klimchitskaya, U. Mohideen, and V. M. Mostepanenko, Theory of the Casimir interaction for graphene-coated substrates using the polarization tensor and comparison with experiment, *Phys. Rev. B* **89**, 115419 (2014).
- [28] G. L. Klimchitskaya and V. M. Mostepanenko, Observability of thermal effects in the Casimir interaction from graphene-coated substrates, *Phys. Rev. A* **89**, 052512 (2014).
- [29] HQ: CSC38/tipless, MicroMash, Watsonville, CA, <http://www.nanoandmore.com>
- [30] Grolltex, San Diego, CA, <http://www.grolltex.com>
- [31] MSE Supplies, Tucson, AZ, <http://www.msesupplies.com>
- [32] Y. Wang, Y. Zheng, X. Xu, E. Dubuisson, Q. Bao, J. Lu, and K. Ping Loh, Electrochemical Delamination of CVD-Grown Graphene Film: Toward the Recyclable Use of Copper Catalyst, *ACS Nano* **5**, 9927 (2011).
- [33] A. Das, S. Pisana, B. Chakraborty, S. Piscanec, S. K. Saha, U. V. Waghmare, K. S. Novoselov, H. R. Krishnamurthy, A. K. Geim, A. C. Ferrari, and A. K. Sood, Monitoring dopants by Raman scattering in an electrochemically top-gated graphene transistor, *Nature Nanotech.* **3**, 210 (2008).
- [34] L. A. Falkovsky, Optical properties of graphene, *J. Phys.: Conf. Series* **129**, 012004 (2008).
- [35] L. A. Falkovsky, Thermodynamics of electron-hole liquids in graphene, *Pis'ma v ZETP* **98**, 183 (2013) [JETP Letters **98**, 161 (2013)].
- [36] Y.-J. Kang, J. Kang, and K. J. Chang, Electronic structure of graphene and doping effect on SiO_2 , *Phys. Rev. B* **78**, 115404 (2008).
- [37] P. Shemella and S. K. Nayak, Electronic structure and band-gap modulation of graphene via substrate surface chemistry, *Appl. Phys. Lett.* **94**, 032101 (2009).
- [38] T. C. Nguyen, M. Otani, and S. Okada, Semiconducting Electronic Property of Graphene Adsorbed on (0001) Surfaces of SiO_2 , *Phys. Rev. Lett.* **106**, 106801 (2011).
- [39] Z. Ao, M. Jiang, Z. Wen and S. Li, Density functional theory calculations on graphene/ $\alpha\text{-SiO}_2$ (0001) interface, *Nanoscale Res. Lett.* **7**, 158 (2012).
- [40] W. Gao, P. Xiao, G. Henkelman, K. M. Liechti, and R. Huang, Interfacial adhesion between graphene and silicon dioxide by density functional theory with van der Waals corrections, *J. Phys. D: Appl. Phys.* **47**, 255301 (2014).
- [41] C.-C. Chang, A. A. Banishev, R. Castillo-Garza, G. L. Klimchitskaya, V. M. Mostepanenko, and U. Mohideen, Gradient of the Casimir force between Au surfaces of a sphere and a plate measured using an atomic force microscope in a frequency-shift technique, *Phys. Rev. B* **85**, 165443 (2012).
- [42] J. Xu, G. L. Klimchitskaya, V. M. Mostepanenko, and U. Mohideen, Reducing detrimental electrostatic effects in Casimir-force measurements and Casimir-force-based microdevices, *Phys. Rev. A* **97**, 032501 (2018).
- [43] M. Liu, J. Xu, G. L. Klimchitskaya, V. M. Mostepanenko, and U. Mohideen, Examining the Casimir puzzle with an upgraded AFM-based technique and advanced surface cleaning, *Phys. Rev. B* **100**, 081406(R) (2019).
- [44] M. Liu, J. Xu, G. L. Klimchitskaya, V. M. Mostepanenko, and U. Mohideen, Precision measurements of the gradient of the Casimir force between ultraclean metallic surfaces at larger separations, *Phys. Rev. A* **100**, 052511 (2019).
- [45] M. Liu, R. Shafer, J. Xu, and U. Mohideen, Elimination of electrostatic forces in precision Casimir force measurements using UV and Argon ion radiation, *Mod. Phys. Lett. A* **35**, 2040001 (2020).
- [46] Bo E. Sernelius, Retarded interactions in graphene systems, *Phys. Rev. B* **85**, 195427 (2012); **89**, 079901(E) (2014).
- [47] M. Bordag, I. V. Fialkovsky, D. M. Gitman, and D. V. Vassilevich, Casimir interaction between a perfect conductor and graphene described by the Dirac model, *Phys. Rev. B* **80**, 245406 (2009).
- [48] I. V. Fialkovsky, V. N. Marachevsky, and D. V. Vassilevich, Finite-temperature Casimir effect for graphene, *Phys. Rev. B* **84**, 035446 (2011).
- [49] M. Bordag, G. L. Klimchitskaya, V. M. Mostepanenko, and V. M. Petrov, Quantum field theoretical description for the reflectivity of graphene, *Phys. Rev. D* **91**, 045037 (2015); **93**, 089907(E) (2016).
- [50] M. Bordag, I. Fialkovskiy, and D. Vassilevich, Enhanced Casimir effect for doped graphene, *Phys. Rev. B* **93**, 075414 (2016); **95**, 119905(E) (2017).
- [51] G. Bimonte, G. L. Klimchitskaya, and V. M. Mostepanenko, Thermal effect in the Casimir force for graphene and graphene-coated substrates: Impact of nonzero mass gap and chemical potential, *Phys. Rev. B* **96**, 115430 (2017).
- [52] E. D. Palik (ed.), *Handbook of Optical Constants of Solids* (Academic Press, New York, 1985).
- [53] C. D. Fosco, F. C. Lombardo, and F. D. Mazzitelli, Proximity force approximation for the Casimir energy as a

- derivative expansion, *Phys. Rev. D* **84**, 105031 (2011).
- [54] G. Bimonte, T. Emig, R. L. Jaffe, and M. Kardar, Casimir forces beyond the proximity force approximation, *Europhys. Lett.* **97**, 50001 (2012).
- [55] G. Bimonte, T. Emig, and M. Kardar, Material dependence of Casimir force: gradient expansion beyond proximity, *Appl. Phys. Lett.* **100**, 074110 (2012).
- [56] G. Bimonte, Going beyond PFA: A precise formula for the sphere-plate Casimir force, *Europhys. Lett.* **118**, 20002 (2017).
- [57] M. Hartmann, G.-L. Ingold, and P. A. Maia Neto, Plasma versus Drude Modeling of the Casimir Force: Beyond the Proximity Force Approximation, *Phys. Rev. Lett.* **119**, 043901 (2017).